

Supercell Size Scaling of Formation Energies of Charged Defects

N.D.M. Hine, K. Frensch, W.M.C. Foulkes and M.W. Finnis

Blackett Laboratory and Thomas Young Centre, Imperial College London, Exhibition Road, London SW7 2AZ, U.K.

Abstract

We present DFT calculations of defect formation energies in alumina, a ceramic oxide considered an archetype for other similar oxides. Combining an existing method for the determination of elemental chemical potentials (as a function of the thermodynamic formation conditions), with a new method for extrapolation to effectively infinite supercell size (removing finite-size errors in electrostatic and elastic energies), we show how the results can be made relatively insensitive to the principal approximations of DFT. These include choices of XC functional and pseudopotential and the supercell in which the calculation is performed. Our results for formation energies are much less sensitive than traditional approaches to these choices, and differ notably from previous results. These are then used as inputs to a new approach to calculating fully ab initio values for expected defect concentrations. From our results of concentrations and activation energies, we are able to explain many previously ill-understood aspects of oxygen and aluminium diffusion in Al_2O_3 .

Defect Formation Energies

Defects are the source of many of the most interesting properties of crystalline solids. Metal oxides are among the most widely-used and studied crystalline solids, so it is clearly important that we are able to understand and simulate defects in such materials. Their uses range from unreactive structural ceramics and refractory materials, to highly efficient fuel cells, catalysts, lasers and many other applications great industrial and technological importance. Aluminium Oxide, Al_2O_3 , is a frequently-studied material that can serve as a prototype for many others of the same structure, and serves to illustrate well many of the challenges of studying such systems, such as low-symmetry structures, complex bonding midway between ionic and covalent, and long-ranged anisotropic interactions.



Figure 1: Three forms of $\alpha\text{-Al}_2\text{O}_3$ with different doping, which affects optical properties: Corundum, Ruby and Sapphire.

The concentration of defects in a material is controlled by the equilibrium conditions under which it was formed or annealed. The Law of Mass Action tells us that concentrations c_i of each species i of defect obey

$$c_i \propto \exp[-\Delta G_f^i/k_B T] \quad (1)$$

The quantity one must calculate is therefore change in Gibbs Free Energy ΔG_f to form the defect. In a DFT calculation, we approximate the non-entropic part of this with the difference in DFT total energies of perfect and defect cells, using the Zhang-Northrup approach [1], so the required formation energy is ΔE_f is

$$\Delta E_f = E_T^{\text{def},q} - E_T^{\text{perf}} - \sum_X \Delta n_X \mu_X + q\mu_e, \quad (2)$$

where Δn_X is the change in number of atoms of species X and μ_X is its chemical potential, and μ_e is the chemical potential of the electron reservoir, expressed as a Fermi energy offset from the valence band maximum: $\mu_e = E_{VBM} + \epsilon_F$. By performing DFT simulations of a supercell of perfect crystal, a supercell containing the defect, and the elemental forms of the constituents, we thus calculate the formation energies of a range of species of defect, such as cation and anion vacancies and interstitials, plus more complex clusters of the above.

Our calculations use ultrasoft pseudopotentials and a plane wave basis set, using the CASTEP code [2]. For the extrapolation to infinite supercell size we pattern the (non-primitive) 30-atom hexagonal cell of Al_2O_3 to a variety of sizes and shapes.

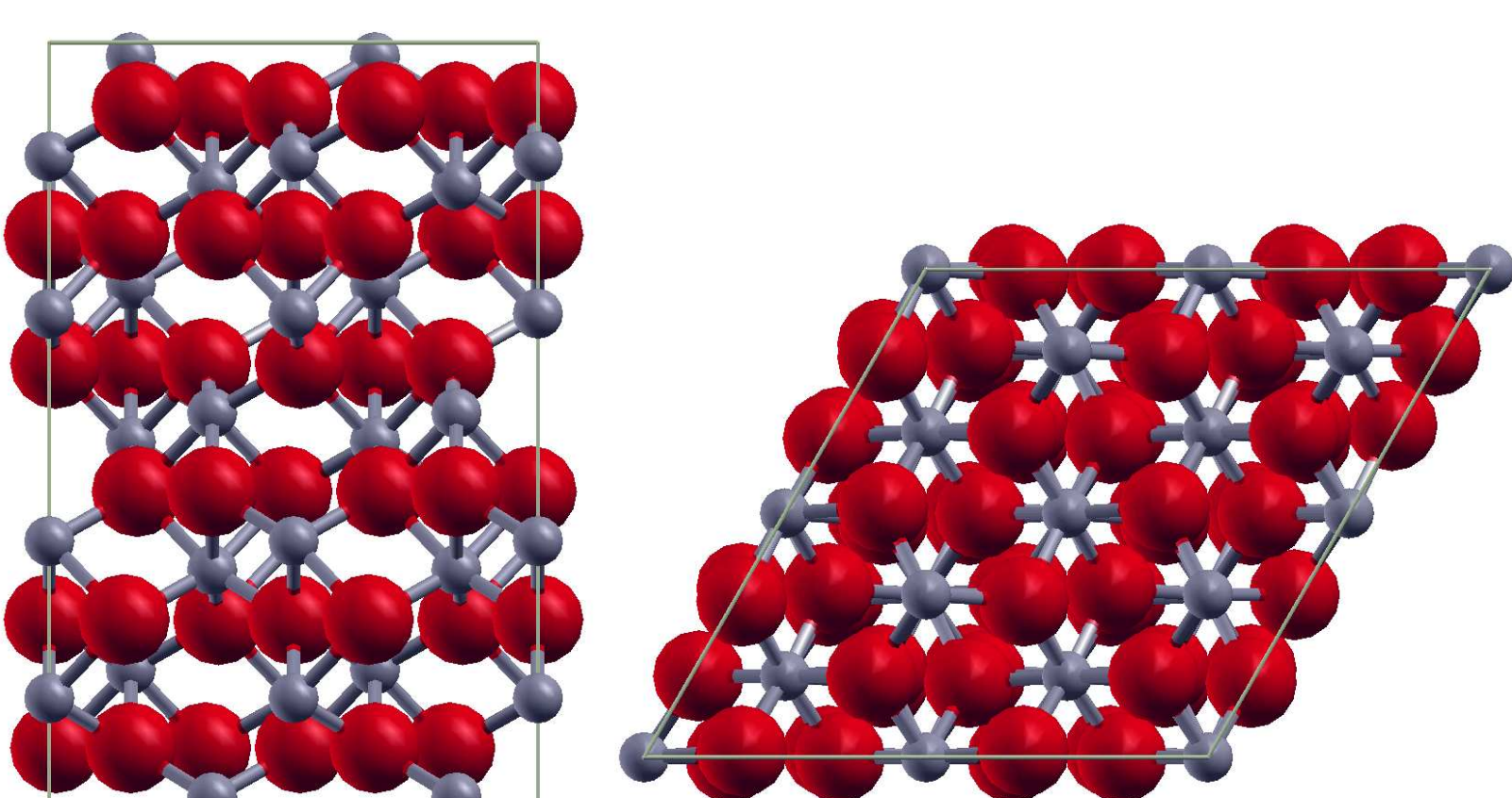


Figure 2: Hexagonal $2 \times 2 \times 1$ supercell of Al_2O_3 . The 2:3 coordination means that Aluminium atoms occupy only 2/3 of the octahedral sites, distorting the structure.

Species Chemical Potentials

Equation 2 contains terms representing the chemical potentials under specific formation conditions of the species present in the crystal, and of the electron reservoir. It is common simply to calculate the range of each μ_X defined by the stability of the solid relative to the elemental phases of each constituent. However, this approach is poor in the case of alumina: not only is the range large due to the large formation energy, in addition the calculation of the total energy of an Oxygen molecule is a challenging one for DFT — producing an answer strongly dependent on choices of XC functional and pseudopotential.

We follow here instead the approach of Finnis, Lozovoi and Alavi [3], which links the chemical potential directly to the formation conditions, and eliminates the use of the unreliable DFT total energy of an Oxygen molecule by using the experimental value of the formation energy of the oxide to complete the cycle. Then, analytic values for an ideal diatomic gas are used to obtain the chemical potentials at specific temperature T and oxygen partial pressure p_{O_2} from the values at STP.

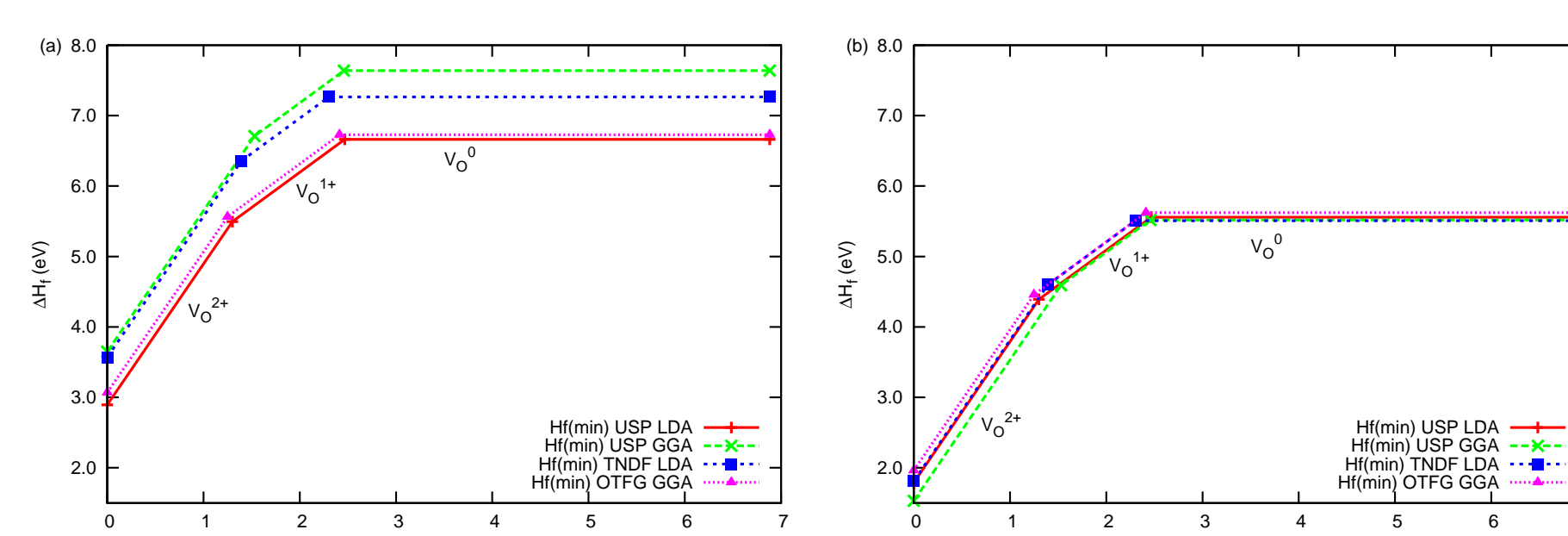


Figure 3: Formation energy of an Oxygen vacancy without (left) and with (right) the above approach to chemical potentials. Note the reduction in the spread of formation energies between different choices of functional and pseudopotential (N.B. the difference in absolute value is arbitrary as it is dependent on the values of p_{O_2} and T used in the determination of μ_{O}).

Supercell Size Scaling

Plane-wave basis sets have great advantages in computational cost and accuracy. However, they are restricted to periodic BC's. One must therefore surround a defect by some finite amount of bulk, and inevitably this leads to errors in the total energy from electrostatic and elastic interactions between periodic replicas of the defect. Previous work on correcting for these interactions, to calculate the formation energy of an isolated defect, has focused on two approaches: analytic correction of the spurious interaction, and extrapolation of finite-cell results to infinite size. Here we employ a new method that mixes elements of both approaches.

The most commonly used correction formula is that of Makov and Payne

$$E_T(L) = E_T(L \rightarrow \infty) - \frac{q^2 \alpha}{2\epsilon L} - \frac{2\pi q Q}{3\epsilon L^3} + \mathcal{O}[L^{-5}] \quad (3)$$

However, neither the experimental or calculated dielectric constant consistently produces a good correction in most solids. Extrapolation techniques instead treat ϵ as a parameter, calculate the total energy at a range of values of L and extrapolate to $L \rightarrow \infty$.

The approach we take here is to note that $\alpha/L \propto v_M$, the Madelung constant, which varies with cell shape as well as size. By varying the different lengths of the supercell independently, and fitting against v_M we can obtain data for a much larger range of cells without going to unfeasibly large simulation cells.

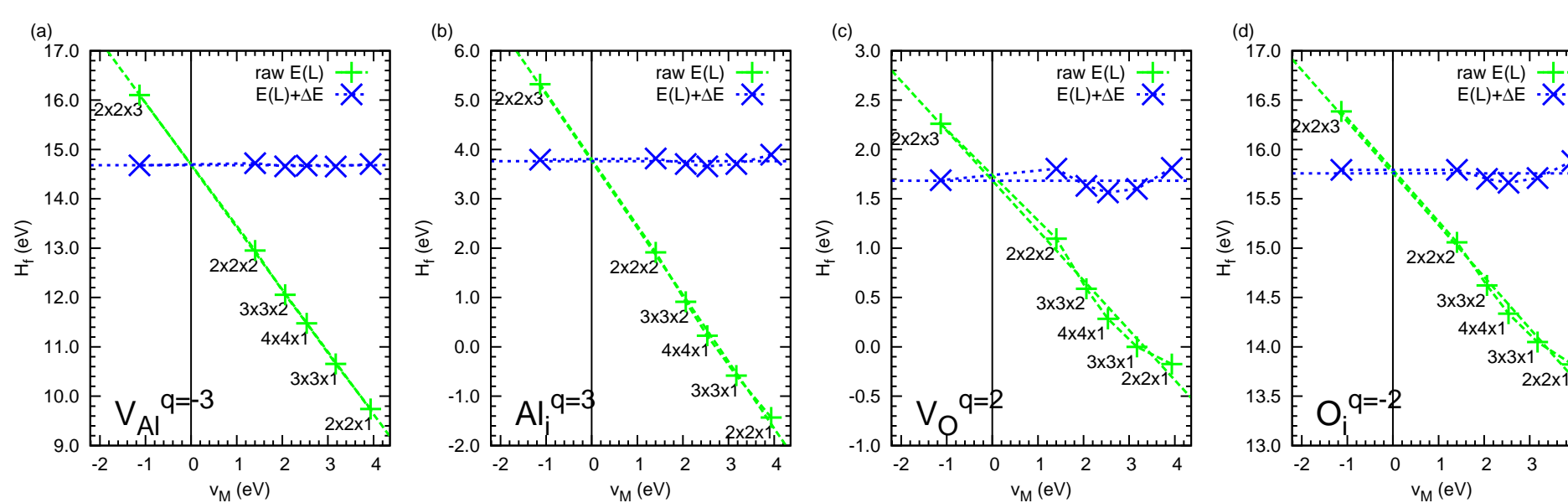


Figure 4: Extrapolation of formation energies of intrinsic defect species to infinite supercell size. The points are from $2 \times 2 \times 1$, $2 \times 2 \times 2$, $2 \times 2 \times 3$, $3 \times 3 \times 1$, $4 \times 4 \times 1$, $3 \times 3 \times 2$ and $4 \times 4 \times 2$ multiples of the hexagonal cell, containing 120, 240, 360, 270, 480, 540, and 960 atoms respectively. Elastic relaxations are not permitted here beyond the 120-atom positions.

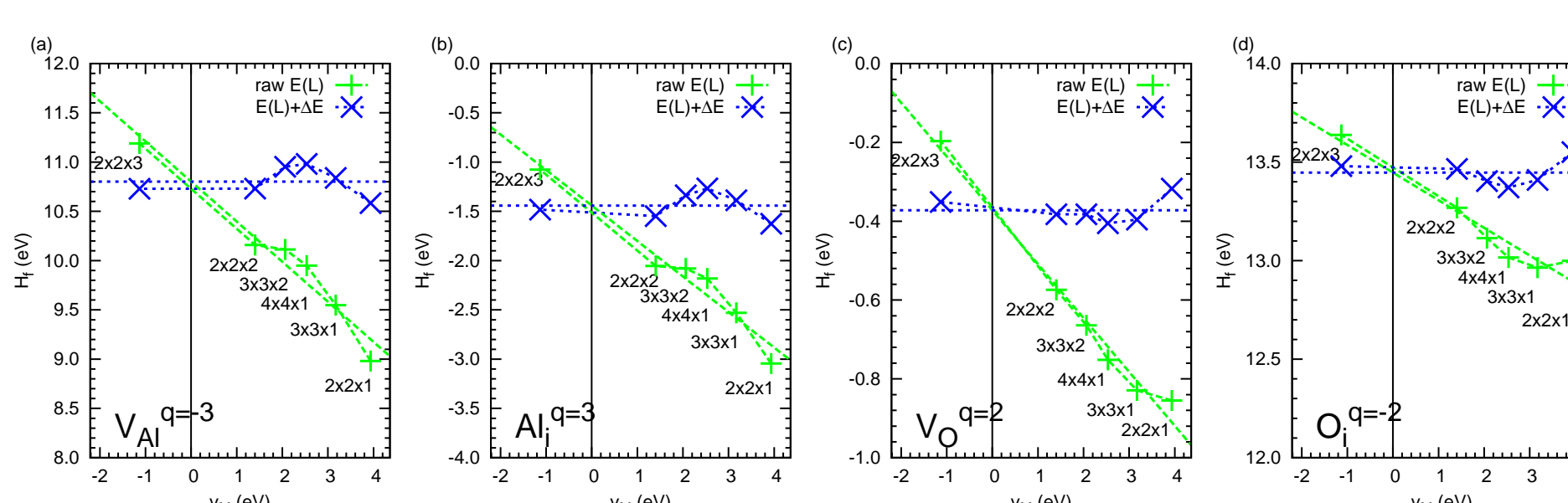


Figure 5: Extrapolation to infinite cell size allowing atomic relaxations, hence including elastic effects. The lines are less straight, but the extrapolation to infinite size remains reliable.

The extrapolation can be carried out with or without elastic relaxations, allowing the electrostatic and elastic effects to be investigated separately. The fitted values of ϵ agree well between different defect species, and are greatly increased when atomic relaxations are included, due to the increased screening by movement of the ions.

Concentrations

These innovations allow us to calculate the formation energies of all the species of intrinsic defect we expect to be common in our system. From these energies, we can calculate the concentrations of these defects in a self-consistent framework.

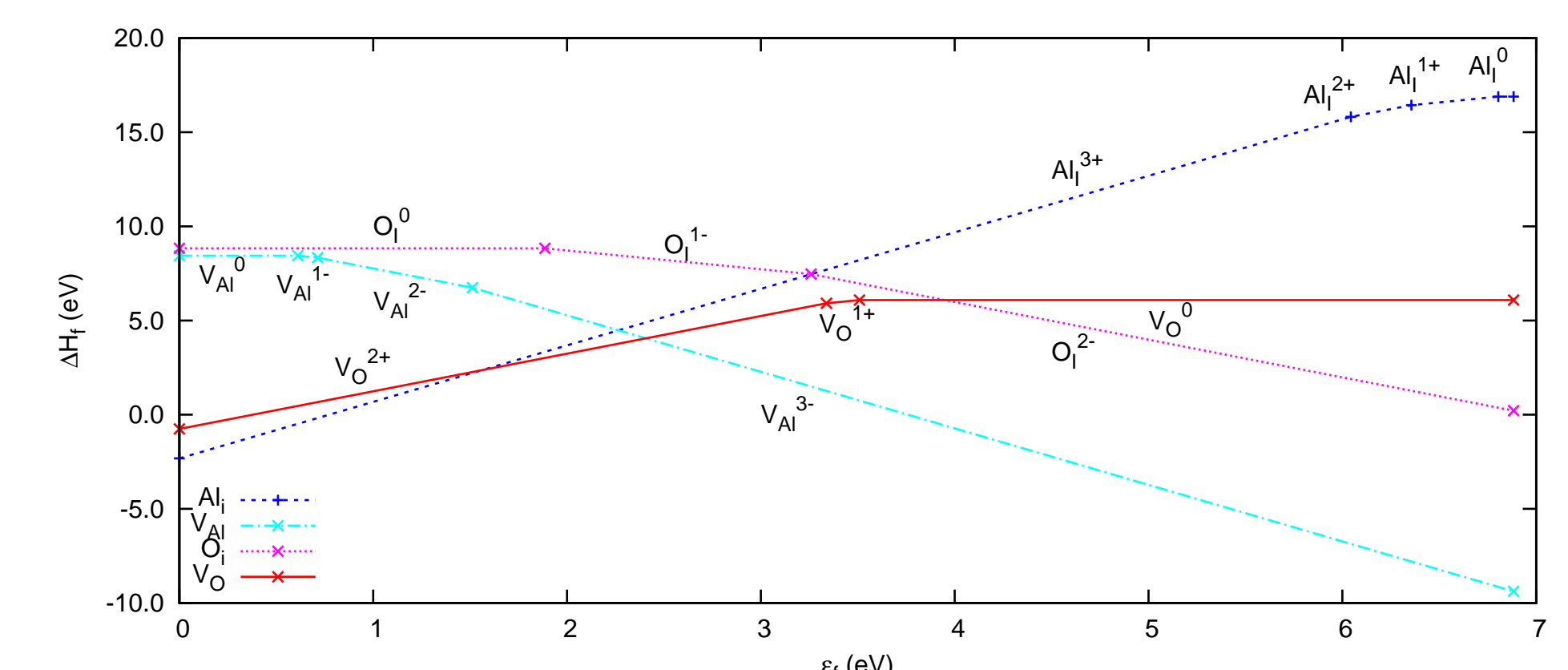


Figure 5: Formation energies of intrinsic defect species as a function of Fermi energy ϵ_F .

Beginning from the Law of Mass Action in Eq. 1, the total Gibbs energy G of a system of Al_2O_3 can be minimised while constraining particle numbers and charge neutrality to give an expression for the concentration of free defects of species i :

$$c_i = p_i \exp\left(-\frac{g_i - \sum_X \mu_X f_i^X + \mu_e q_i}{k_B T}\right). \quad (4)$$

μ_X is the chemical potential of element X , f_i^X the number of atoms of X in a molecular unit containing a single defect of type i , q_i the charge on such a molecular unit, and p_i the number of permutations of sites and orientations of defect i . The constraint of charge neutrality ensures that the net charge $Q_i = \sum_0 c_i q_i$ of the native defects per formula unit cancels the net charge of dopants per formula unit, Q_d . This draws an important parallel between theory and experiment. Q_d is the total charge of all dopants present, including those contained in clusters and those with bound native defects. Care must be taken interpreting Q_d in terms of actual dopant atom concentrations as the charge provided may well be bound up in clusters not included in the present formulation.

We find the value of μ_{O} equivalent to particular formation conditions T , p_{O_2} , and the corresponding $\mu_{\text{Al}} = \frac{1}{2}(\mu_{\text{Al}_2\text{O}_3} - 3\mu_{\frac{1}{2}\text{O}_2})$, then solve Eq. 4 iteratively, adjusting μ_e until the charge balance $Q_i = -Q_d$ is obtained. This yields the concentrations of individual defect species as functions of T , p_{O_2} and Q_d , and also gives a self-consistent value of μ_e , and thus the Fermi level. ϵ_F will shift for different levels of net doping as charge-compensating defects are created to balance Q_d , and, for Al_2O_3 , it is found that ϵ_F is then confined to a region of ca. 2eV within the band gap.

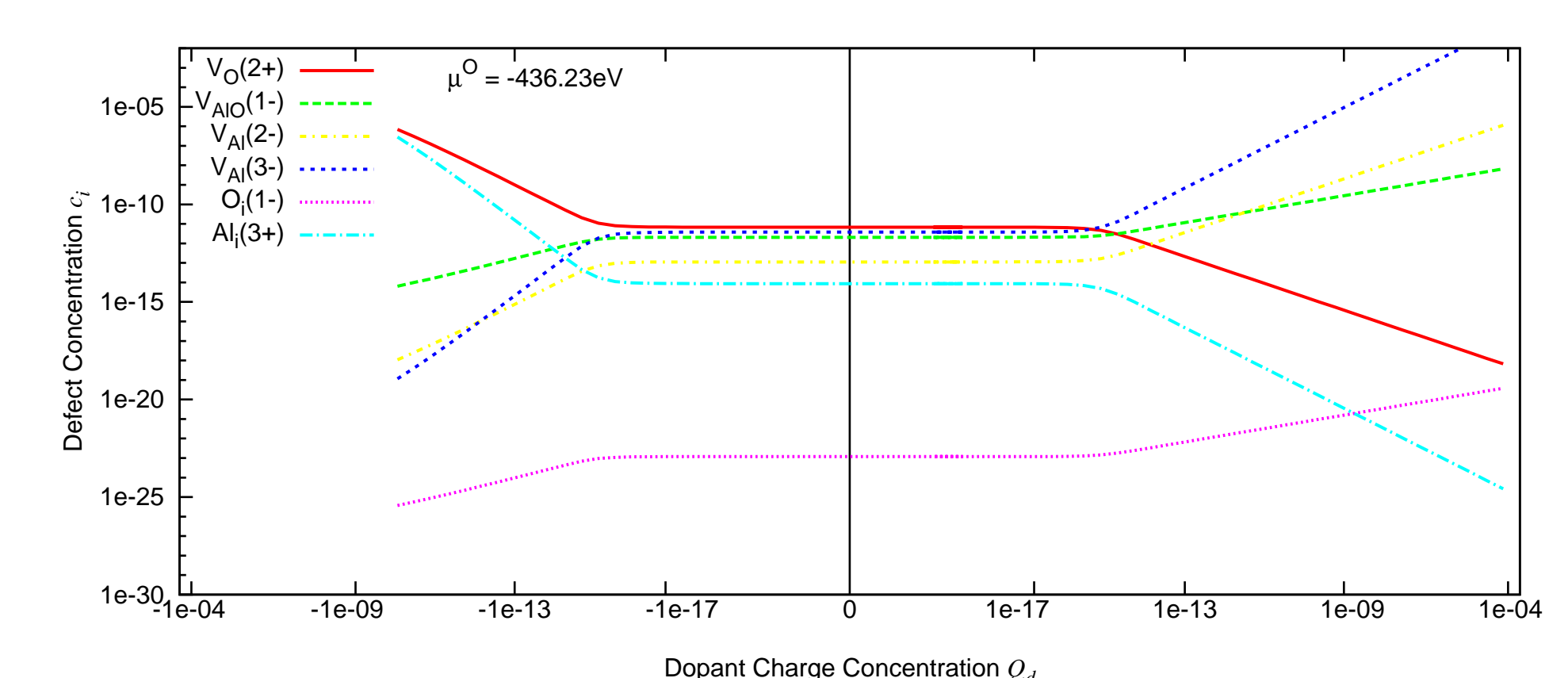


Figure 6: Defect concentrations $[X]$ as a function of net dopant charge concentration Q_d on a log-log plot at $T = 1750\text{K}$, $p_{\text{O}_2}/p^0 = 0.2$. For defect species of low relative concentrations, only the most abundant charge state is shown.

These changes in ϵ_F dictate changes in the formation energies, and thus the activation energies for diffusion $Q_i^{\text{act}} = \Delta E_{\text{mig}} + \Delta E_f$. With these results, we can explain many of the puzzles of diffusion in this material. We can show that the remarkable confluence of bulk diffusion data in Al_2O_3 , despite numerous experimental difficulties and differences between sample impurity levels, owes in large part to the confinement of ϵ_F to a strict regime within the band gap and the higher than previously thought intrinsic levels of defects. Together, these cause ϵ_F to remain almost constant across wide ranges of doping, leading to constant diffusion coefficients.

Conclusions

We present an approach to calculating defect formation energies and defect concentrations that allows one to predict, with no empirical input, a self-consistent set of concentrations for all the intrinsic defects under consideration, taking only the thermodynamic variables describing the formation conditions as inputs. This method has diverse applications across materials science, as in very many fields a full understanding of defect concentrations is crucial to improving material properties.

References

- [1] S. B. Zhang and J. E. Northrup, Phys. Rev. Lett. **67**, 2339 (1991).
- [2] S. J. Clark *et al*, Zeitschrift für Kristallographie, **220**, 567 (2005).
- [3] M. W. Finnis, A. Y. Lozovoi and A. Alavi, Annu. Rev. Mater. Res. **35**, 167 (2005).